Structural studies of 2-(3′,4′-dihydroxyphenyl)-7-β-D-glucopyranos-1-*O*-yl-8-hydroxychroman-4-one in the liquid and solid states by means of 2D NMR spectroscopy and DFT calculations

S. Olejniczak,[a] K. Ganicz,[a] M. Tomczykowa,[b] J. Gudej[b] and M. J. Potrzebowski[a]

[a] *Polish Academy of Sciences, Center of Molecular and Macromolecular Studies, 90-363 Łódź, Sienkiewicza 112, Poland. E-mail: marekpot@bilbo.cbmm.lodz.pl*
[b] *Medical Academy of Białystok, Department of Pharmacognosy, 15-230 Białystok, Mickiewicza 2a, Poland*

Received (in Cambridge, UK) 7th March 2002, Accepted 15th April 2002
First published as an Advance Article on the web 10th May 2002

Homo- and heteronuclear correlated spectroscopy in the liquid phase and the PASS-2D NMR technique in the solid state were applied to the identification and structural studies of the flavanone 2-(3′,4′-dihydroxyphenyl)-7-β-D-glucopyranos-1-*O*-yl-8-hydroxychroman-4-one **1**. The principal elements of the ^{13}C chemical shift tensor were established and verified by DFT GIAO calculations. Analysis of the ^{13}C δ_{ii} and comparison with the theoretical shielding parameters calculated for different conformers of **1** in a vacuum were carried out to choose the most reliable geometry in the solid state.

1 Introduction

Flavonoids belong to an important class of biological species, which are secondary products of plant metabolism. These compounds, including flavonols, flavonones and isoflavonones represent a significant source of antioxidants[1] and exhibit antiallergenic, antiviral, radical scavenging or antiinflammatory activities. They are also capable of modulating the activity of enzymes. Knowledge of the molecular structure of flavonoids is crucial in understanding their biological activity. These activities have been the subject of many studies and reports.[2] Although important structure–activity relationships for the antioxidant properties have been established there is no simple relationship between, for example, radical scavenging activity and conformation.

Recently, Wawer and Zielińska[3] reported solution and solid state ^{13}C NMR data for selected flavonoids. NMR spectroscopy was presented as a fast and non-destructive method to identify compounds of biological interest and as an efficient probe for studying the orientation of the hydroxy groups and the effect of hydrogen bonding. The isotropic values (δ_{iso}) of ^{13}C chemical shifts in the liquid and solid phases were established and discussed. It is well known however, that detailed information about the geometry and nature of inter- and/or intramolecular contacts can be obtained from inspection of the principal elements of the ^{13}C chemical shift tensor δ_{ii}.[4] To the best of our knowledge, such a potential has not been explored due to problems with the interpretation of heavily overlapping 1D NMR spectra for this class of compounds.

In this paper we illustrate the power of 2D NMR techniques in both the liquid and solid states in the structural studies of flavonoids, employing, as a model carbohydrate derivative of flavanone, 2-(3′,4′-dihydroxyphenyl)-7-β-D-glucopyranos-1-*O*-yl-8-hydroxychroman-4-one **1** obtained from *Bidens tripartita*. Compound **1** was isolated by Serbin and co-workers,[5] but its molecular structure has never been investigated and confirmed by advanced NMR spectroscopy.

Our project was carried out in several stages. First, the full assignment of the solution structure of **1** by means of 1D and 2D NMR techniques was done. Secondly, the ^{13}C δ_{iso} parameters in the solid phase were established employing the CP/MAS technique under fast sample spinning (10 kHz). Thirdly, an attempt to find the ^{13}C δ_{ii} parameters for **1**, difficulties with the analysis of CP/MAS slow sample spinning (2 kHz) spectra and the power of PASS-2D (**P**hase **A**djusted **S**pinning **S**idebands) sequences[6,7] in the interpretation of overlapping systems is discussed. Finally, application of the quantum chemical approach in the elucidation of the ^{13}C δ_{ii} parameters (DFT GIAO calculations), their correlation to experimental data and comparative analysis of ^{13}C δ_{ii} parameters in both the solid phase and in a vacuum are presented.

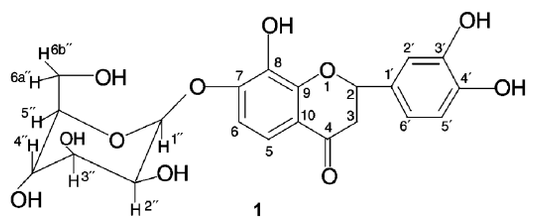

1

2 Results and discussion

^{1}H and ^{13}C NMR studies of 1 in solution

The one- and two-dimensional ^{1}H and ^{13}C NMR spectra were analyzed in order to obtain the complete assignment of proton and carbon chemical shifts and to elucidate the structure of **1**. In some experiments we have taken advantage of the pulse field gradient (PFG) system to reduce the time of measurement and improve the quality of spectra. The ^{1}H and ^{13}C chemical shifts as well as proton–proton *J* coupling constants were established by means of ^{1}H–^{1}H PFG COSY (**Co**rrelation **S**pectroscopy), ^{1}H–^{1}H PFG TOCSY (**To**tally **C**orrelated **S**pectroscopy), ^{1}H–^{13}C PFG HMQC (**H**eteronuclear **M**ultiple **Q**uantum **C**oherence) and ^{1}H–^{13}C PFG HMBC (**H**eteronuclear **M**ultiple **B**onds **C**oherence) experiments. The HMBC experiment was optimized for $^{3}J = 5$ Hz. The ^{1}H chemical shifts and the values of the geminal (^{2}J) and vicinal (^{3}J) coupling constants for **1** are given in Table 1. From inspection of the ^{1}H NMR data it is apparent that the carbohydrate substituent is attached to the C7 carbon of the flavonone ring. Further information was

DOI: 10.1039/b202414b

Table 1 ^{1}H NMR (500 MHz) data for 2-(3′,4′-dihydroxyphenyl)-7-β-D-glucopyranos-1-*O*-yl-8-hydroxychroman-4-one

Proton	δ (DMSO-d_6) (ppm)	*J*/Hz
H2	5.40 (dd)	$^{3}J_{(H2–H3a)}$ = 12.2
H3a	2.70 (dd)	$^{2}J_{(H3a–H3e)}$ = 16.8
H3e	2.60 (dd)	$^{3}J_{(H3e–H2)}$ = 2.6
H5	7.23 (d)	$^{3}J_{(H5–H6)}$ = 8.8
H6	6.86 (d)	—
H2′	6.92 (d)	—
H5′	6.78 (d)	$^{3}J_{(H5′–H6′)}$ = 8.8
H6′	6.75 (d)	—
H1″	4.81 (d)	$^{3}J_{(H1″–H2″)}$ = 7.4
H2″	3.47 (dd)	$^{3}J_{(H2″–H3″)}$ = 12.2
H3″	3.29 (dd)	$^{3}J_{(H3″–H4″)}$ = 3.5
H4″	3.33 (dd)	$^{3}J_{(H4″–H5″)}$ = 9.5
H5″	3.28 (dd)	$^{3}J_{(H5″–H6a″)}$ = 2.2
H6a″	3.71 (d)	$^{3}J_{(H5″–H6b″)}$ = 1.8
H6b″	3.2 (d)	$^{2}J_{(H6a″–H6b″)}$ = 11.8
C8–OH	8.5	—
C3′–OH	9.0	—
C4′–OH	9.0	—
C2″–OH	5.4	—
C3″–OH	5.1	—
C4″–OH	5.1	—
C6″–OH	4.6	—

Table 2 ^{13}C NMR (125 MHz) data for 2-(3′,4′-dihydroxyphenyl)-7-β-D-glucopyranos-1-*O*-yl-8-hydroxychroman-4-one

Carbon	δ (DMSO-d_6) (ppm)
C2	79.3
C3	43.4
C4	191.2
C5	116.6
C6	109.0
C7	150.7
C8	135.1
C9	150.7
C10	116.6
C1′	129.9
C2′	114.5
C3′	145.6
C4′	145.2
C5′	115.3
C6′	118.0
C1″	101.5
C2″	75.7
C3″	73.2
C4″	69.7
C5″	77.3
C6″	60.6

obtained from ^{13}C NMR (Table 2). The assignment of the quaternary carbons and their long range correlation with protons (^{1}H–^{13}C HMBC) was a crucial point in the structure elucidation of **1**.

Solid state NMR studies of 1

We were attracted to this part of the project by the prospect of the analysis of the ^{13}C δ_{ii} data for **1**, inspection of the anisotropic values for the chemical shift tensors and a correlation of the principal elements with the molecular structure. For this purpose, the approach, which covers high-resolution solid state NMR and theoretical calculations is found to be the method of choice.

The ^{13}C CP/MAS spectrum of **1** recorded at 10 kHz with RAMP[8] shape cross-polarization and TPPM decoupling[9] is shown in Fig. 1a. An assignment of the isotropic chemical shifts for **1** was achieved by comparing the data with those obtained in the liquid phase.

For rotating solids, ^{13}C δ_{ii} parameters can be obtained from an analysis of spinning side-band intensities employing for instance the graphical method *via* deconvolution of spectra recorded at a low spinning rate. For the sample under investigation, the spinning rate should be in the range of 2–3 kHz, to obtain a spectrum with a sufficient number of sidebands for further calculations. As we found, in the case of **1** which consists of 21 carbon atoms, the deconvolution procedure is not an easy task. At a low spinning speed (Fig. 1b) the overlap between different spinning sidebands manifolds and analysis of the spectrum is ambiguous. The separation of isotropic and anisotropic parts of the spectra with heavily overlapping systems is still a challenge for solid state NMR spectroscopy. There are several approaches which enable the achievement of this goal. Pines and co-workers introduced VACSY methodology, which with great success was employed to analyze a tyrosine sample.[10] Grant's group, by modifying the Gan's MAT (Magic Angle Turning) approach has revealed the power of PHORMAT and FIREMAT pulse sequences in structural studies of complex, organic compounds.[11,12] The merits of the TOSS-de-TOSS experiment were presented by Kolbert and Griffin.[13] Recently Anzutkin *et al.* introduced the PASS 2D sequence,[6,7] which compared to previous techniques offers good sensitivity and does not require any hardware modifications or a special probehead. A detailed explanation of the PASS-2D pulse sequence, its performance, a *Mathematica* routine to generate a set of PASS solutions, and the data processing can be found elsewhere.[6,14]

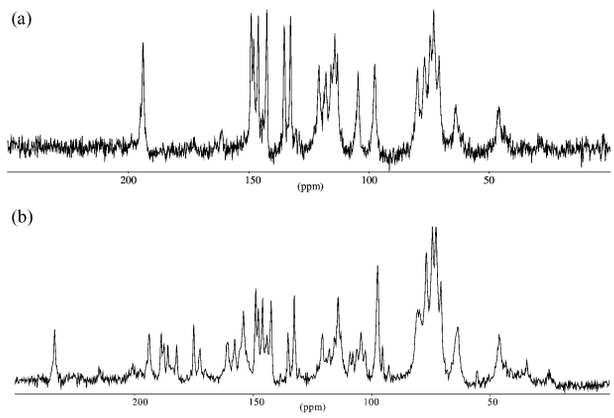

Fig. 1 75.46 MHz ^{1}H–^{13}C CP/MAS spectra of **1** recorded at 10 kHz (a) and 3 kHz (b) with RAMP shape cross-polarization and TPPM decoupling. The spectra have 4K data points with 20 Hz line broadening.

Fig. 2 displays the PASS-2D spectrum of **1**, recorded with a spinning rate of 2 kHz. Both the carbonyl group and aromatic atoms are characterized by a large chemical shift anisotropy (CSA) and under slow sample spinning the spectrum obtained presents a complex pattern. By proper data shearing (Fig. 3) it is possible to separate spinning sidebands for each carbon and by employing a calculation procedure establish the ^{13}C δ_{ii} parameters. It is clear from such a presentation that the F2 projection corresponds to the TOSS[15] spectrum while F1 represents CSA. In our project to calculate the ^{13}C δ_{ii} parameters we decided to use the graphical method of Herzfeld–Berger and the WINMAS program.[16,17] However, such an approach requires that calculated data be tested for accuracy. We verified this methodology by employing L-histidine hydrochloride monohydrate **2** as a reference sample. The ^{13}C δ_{ii} elements for **2** have been published elsewhere.[18]

Fig. 4a shows a contour plot of the PASS-2D spectrum of sample **2**. The 1D spectra of carbons 0, 2, 4 and 5 (for numbering system see inset in Fig. 4) taken from columns of the 2D spectrum and appropriate simulated spectra are presented in Fig. 4b. The accuracy of these calculations was confirmed by a comparison of the ^{13}C CP/MAS spectrum and a simulated spectrum with ^{13}C δ_{ii} parameters taken from the PASS-2D experiment (Fig. 5). The values of the ^{13}C δ_{ii} are presented in

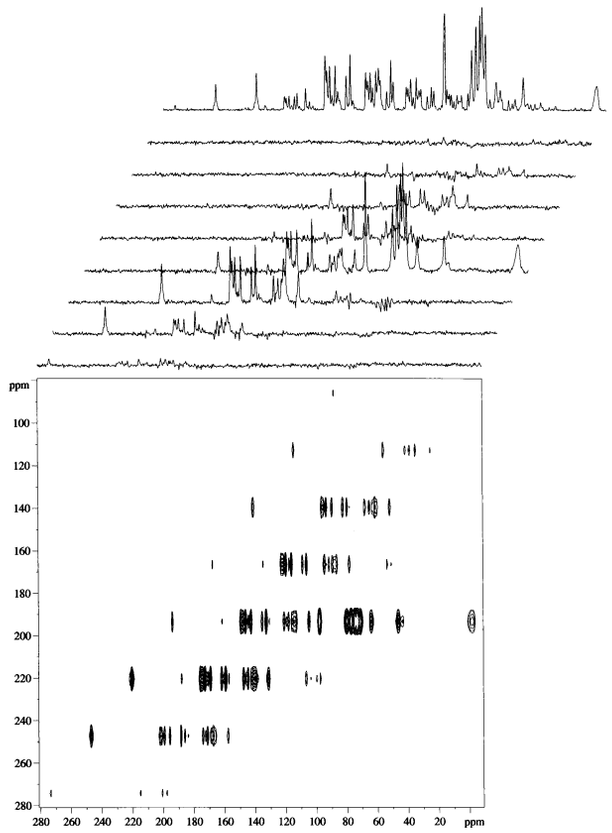

Fig. 2 PASS-2D spectrum of **1** recorded with a spinning rate of 2 kHz.

Fig. 5. The power of these 2D techniques is apparent. Even the signal of the C4 carbon, which at 2 kHz in the ^{13}C CP/MAS spectrum is overlapped by the spinning sidebands of the carboxy group, can be easily analyzed. The very good correlation with the reference data and the high fidelity of the experimental and calculated spectra enabled us to use this approach in the analysis of the more complex system of sample **1**.

The experimental and the best-fitting simulated 1D spinning CSA sideband patterns for selected carbons of **1** are shown in Fig. 6. The sidebands of the carbonyl C4 group are clear cut and easy to analyze. The anisotropy of the C4 carbon is the largest compared to the other resonances. The aromatic signals are well separated and the intensity of the sidebands can be established. Having such information we were in a position to calculate the ^{13}C δ_{ii} parameters for **1**. The ^{13}C shielding values are collected in Table 3.

DFT GIAO calculations

The value and orientation of the principal elements of the chemical shift tensor with respect to the molecular frame is a source of important information about the nature of NMR shielding and intermolecular contacts. The orientation remains hidden by MAS NMR investigations. This missing information can be obtained experimentally by an NMR goniometer measurement of single crystals or theoretically by quantum chemical nuclear shielding calculations. The latter approach was employed in our project. There are a number of methods available for computing the NMR parameters.[19,20] In this work we used the density functional method (DFT) to calculate the principal elements of the ^{13}C shielding tensor σ_{ii}. There is no X-ray diffraction data for **1** in the Cambridge Structural Database. As an input file for our calculations we used the geometry obtained by molecular modeling and optimized this with the B3PW91 functional and 6-311G** base. Since in the previous section we discussed CSA only for the flavonone part of **1**, in order to reduce the time required for the calculations we replaced the sugar molecule of **1** with a methyl group obtaining model **1a**. As we revealed in our previous paper such an approach has no substantial influence on the quality of calculation and the values of theoretical shielding parameters.[21] Although the simplifying procedure was employed, a problem with finding the energy minimum for **1a** occurred due to the large flexibility of the heterocyclic ring and the low barrier of phenyl group rotation around the C1′–C2 bond. The conformational and dynamic effects occurring in chroman derivatives have recently been discussed elsewhere.[22] The stereochemistry of the chiral centers of flavanones and isoflavanones is a matter which has received considerable attention and is still a challenge in structural chemistry.[23] In our calculations, for **1a** we assumed *S* absolute configuration at the C2 chiral center by analogy with other flavanones with known stereochemistry.[24]

Our preliminary results showed that in a vacuum, perpendicular alignment of the two phenyl rings represents the optimal conformation of **1a**. This result does not have to be consistent with the preferred structure in the solid phase. As concluded from X-ray data a similar class of compounds, flavonoids, tend to form flat structures organized into layers due to strong aromatic–aromatic interactions.[25] In order to establish

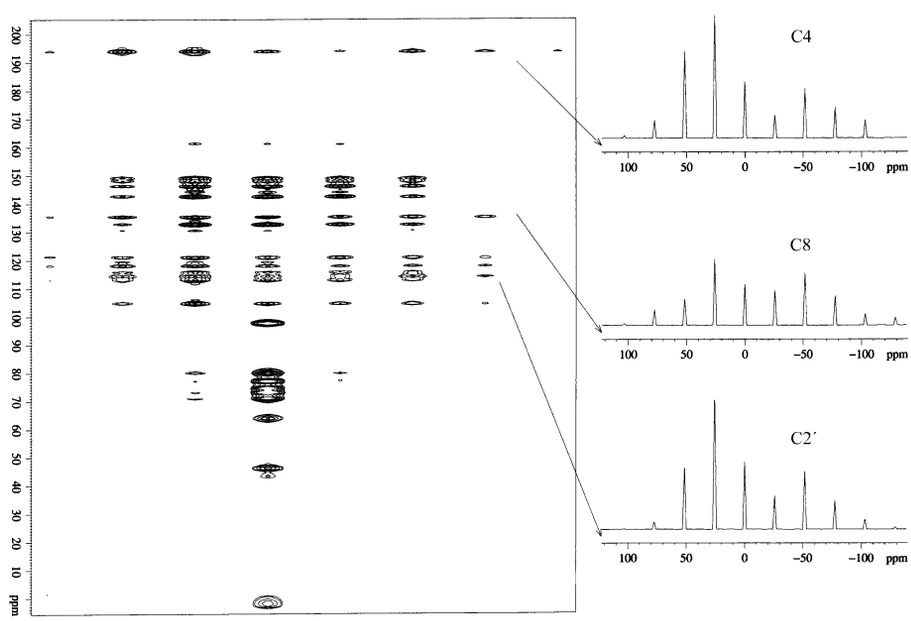

Fig. 3 Separated spinning sideband patterns for the selected C4, C8 and C2′ carbons of **1**.

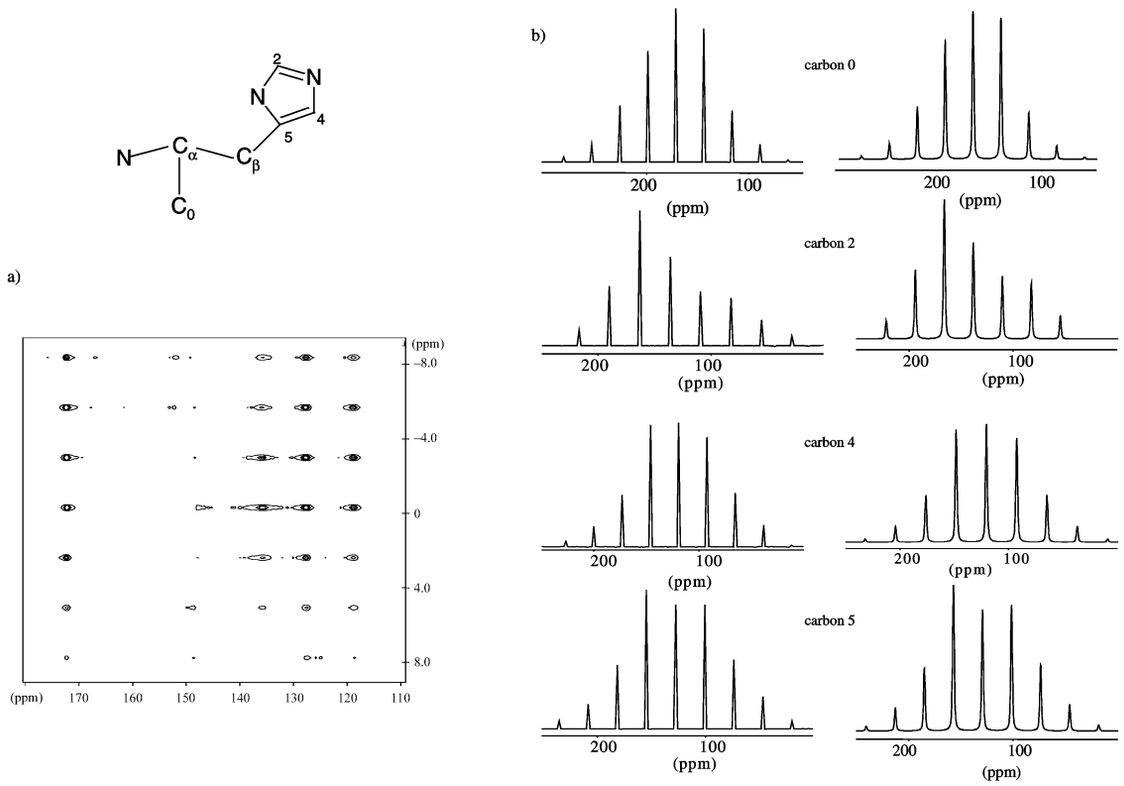

Fig. 4 a) Contour plot of a PASS-2D spectrum of L-histidine hydrochloride monohydrate **2**, b) 1D experimental and simulated spectra of carbons C0, C2, C4 and C5 of **2** taken from a 2D spectrum.

carbon	δ_{iso} (ppm)	δ_{11} (ppm)	δ_{22} (ppm)	δ_{33} (ppm)
0	172.5	236	171	110
2	136.0	212	156	42
4	119.0	199	111	48
5	127.7	202	129	53

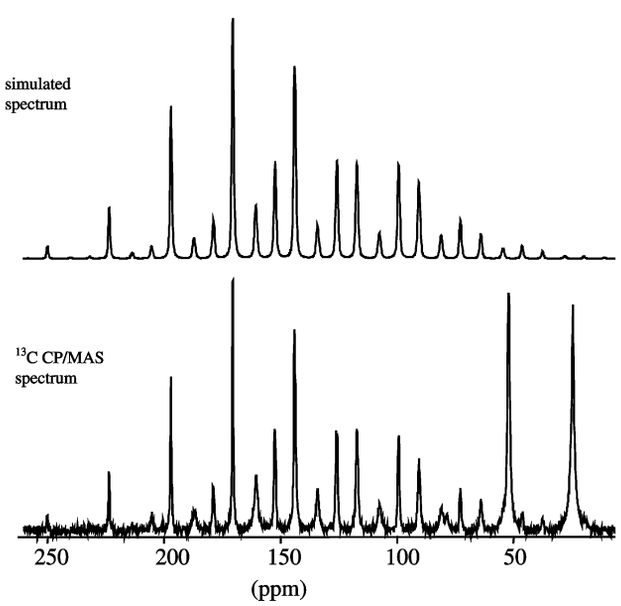

Fig. 5 Comparison of the simulated and the experimental ^{13}C CP/MAS spectra of **2**, α and β carbons are omitted.

the consistency between the theoretical calculations and the experimental results we carried out calculations for **1a** with frozen rotation around the C1′–C2 bond incrementing the appropriate torsion angle by approximately 10°. For each optimized geometry the ^{13}C σ_{ii} parameters were established. Fig. 7a shows the changes of SCF energy as a function of the O–C2–C1′–C6′ torsion angle. From this plot it is apparent that there are two local energy minima for the conformation as shown in Fig.8. Fig. 7b presents the changes of R^2 standard deviation values[26] as a function of O–C2–C1′–C6′. It is worth noting that the relationship of the theoretical shielding σ_{ii} *versus* the experimental chemical shift δ_{ii} parameters show a similar trend, but the best fit (lowest energy, highest R^2) is found for the first minimum. Such information provides an important hint as to the favored solid state geometry.

Table 3 ^{13}C chemical shift parameters for **1** obtained by means of the PASS-2D methodology

Carbon	δ_{iso} (ppm)	δ_{11} (ppm)	δ_{22} (ppm)	δ_{33} (ppm)
C4	194.2	269.8	235.2	77.6
C5	117.6	205.5	142.3	5.0
C6	104.6	169.0	127.9	16.9
C7	149.2	207.4	171.4	68.8
C8	135.4	217.5	164.4	24.4
C9	148.2	211.2	161.7	71.7
C10	114.4	189.6	130.5	23.0
C1′	132.8	177.7	161.6	58.9
C2′	113.6	179.5	132.6	28.4
C3′	146.3	213.0	152.4	73.5
C4′	142.6	209.5	149.7	68.7
C5′	114.0	169.7	157.3	15.3
C6′	120.3	203.6	133.6	24.0

The best fitted (R^2 = 0.98) theoretical ^{13}C chemical shielding parameters established by means of the DFT GIAO method for **1a** are collected in Table 4. Fig. 9a shows the plot of ^{13}C σ_{ii} *versus* δ_{ii}. Correlation of the experimental isotropic and theoretical shielding parameters is presented in Fig. 9b. Inspection of Fig. 9a reveals that the scatter of experimental and theoretical points differs in each part of the plot. For δ_{11}/σ_{33} the R^2 is 0.96, while for δ_{22}/σ_{22} and δ_{33}/σ_{11} R^2 is 0.80 and 0.83, respectively. These discrepancies could be due to intermolecular effects, which were not considered in our calculations.

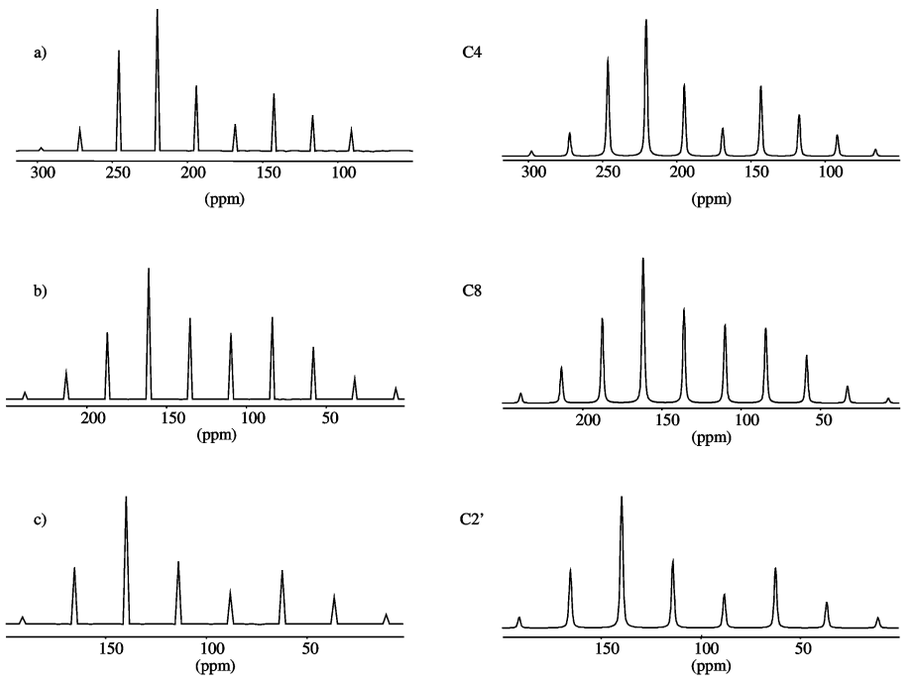

Fig. 6 Experimental and best fitting simulated 1D spinning CSA sideband patterns for selected carbons of **1** a) C4, b) C8 and c) C2′.

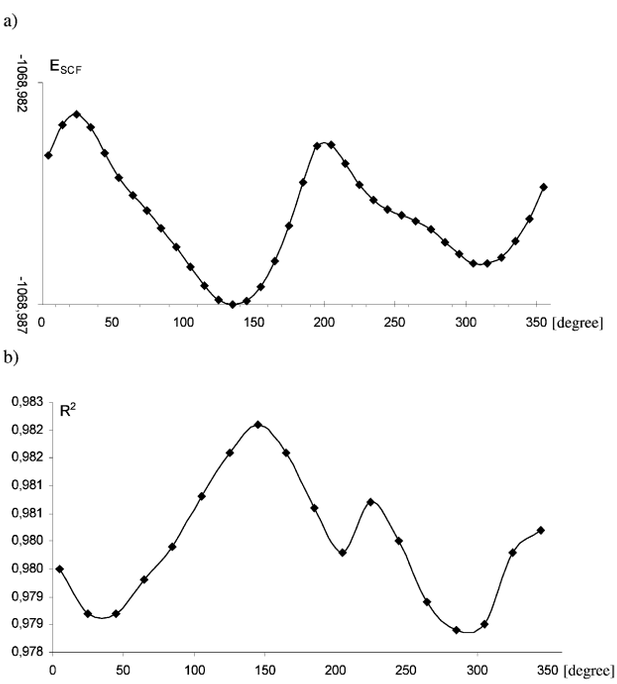

Fig. 7 a) Changes of SCF energy as a function of the O–C2–C1′–C6′ torsion angle. b) Changes of R^2 values as a function of the angle O–C2–C1′–C6′

The orientation of the principal elements of the chemical shift tensors with respect to the molecular frame of **1a** is displayed in Fig. 10 and given in Table 5. The δ_{33} parameter of C4 is perpendicular to the carboxy plane while δ_{22} elements lie along the C=O bond. For six-membered aromatic rings the most shielded element δ_{33} is perpendicular to the plane of the ring and the least shielded one (δ_{11}) is directed to the proton or the group connected to the carbon. The δ_{22} parameter is aligned in the plane of the aromatic system and therefore the distribution of π-electrons determines its value. Knowing the orientation of ^{13}C δ_{ii} parameters with respect to the molecular frame and considering the differences between the experimental and theoretical δ_{22} and δ_{33} elements, it's clear that strong aromatic–aromatic interactions and hydrogen bonding (C=O group) determine the molecular packing of sample **1** in the solid phase.

Table 4 The best fitted (R^2 = 0.98) theoretical ^{13}C chemical shielding parameters established by means of the DFT GIAO method for **1**

	B3PW91/6-311++G**			
Carbon	σ_{iso}	σ_{11}	σ_{22}	σ_{33}
2	101.42	69.97	89.01	145.27
3	143.82	134.35	136.46	160.65
4	−13.34	−102.01	−40.43	102.43
5	62.04	−38.70	40.19	184.64
6	77.82	−7.72	65.01	176.18
7	26.78	−30.14	1.20	109.28
8	45.93	0.17	18.99	118.63
9	30.29	−21.49	4.61	107.77
10	66.93	2.71	33.55	164.54
1′	50.83	−36.30	29.27	159.50
2′	73.53	−5.87	65.72	160.75
3′	38.32	−28.21	27.71	115.48
4′	34.12	−30.37	15.29	117.45
5′	65.32	−19.76	48.48	167.26
6′	58.63	−42.39	45.25	173.03

In conclusion, we have presented a new approach to the analysis of PASS-2D spectra based on the standard BRUKER WINMAS program. As we have revealed this methodology gives accurate values of ^{13}C principal elements of chemical shift tensors and can be considered an alternative way to the approach suggested by Anzutkin *et al.*[6,7,14] Moreover, the analysis of ^{13}C δ_{ii} values and their comparison with theoretical shielding parameters calculated for different conformers of **1** in a vacuum can be employed to choose the most reliable geometry in the solid state.

3 Experimental

General experimental procedures

Solution state NMR spectra were recorded on a Bruker Avance DRX 500 spectrometer operating at 500.1300 MHz for ^1H and 125.2578 MHz for ^{13}C. For all experiments original Bruker pulse programs were used. The chemical shift of the DMSO signal was used as a reference (δ = 2.49 ppm for ^1H and δ = 39.5 ppm for ^{13}C). The spectrometer was equipped with a pulse field

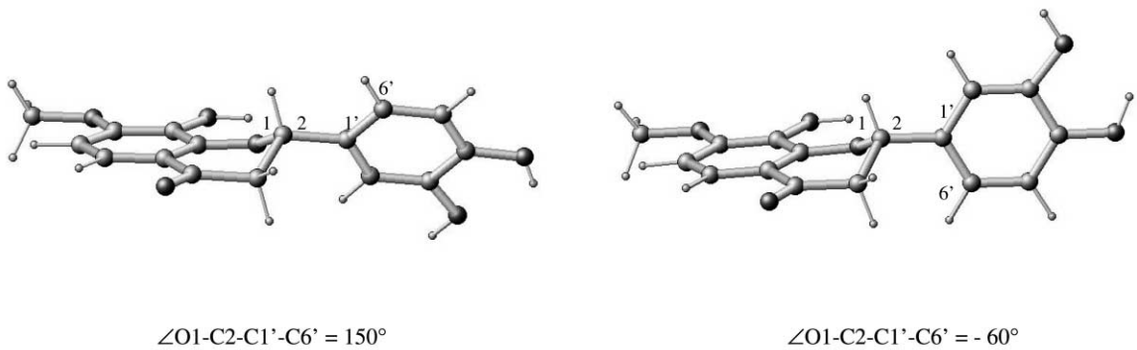

Fig. 8

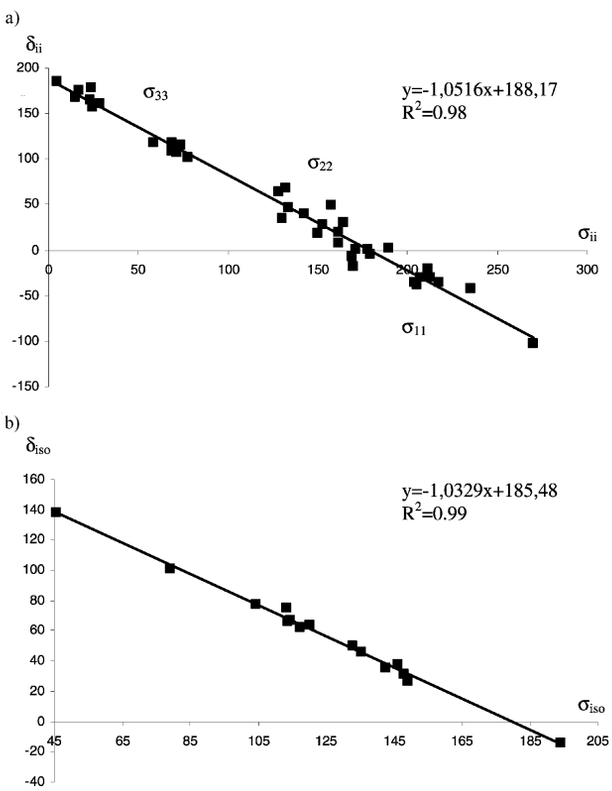

Fig. 9 a) Correlation of the experimental isotropic and theoretical shielding parameters. b) Correlation between ^{13}C shielding parameters σ_{ii} and the chemical shift δ_{ii} parameters.

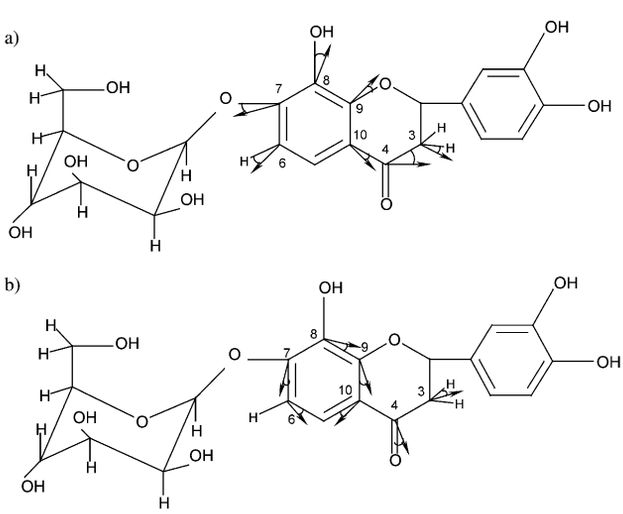

Fig. 10 Location of the δ_{11} (a) and δ_{22} (b) components of the chemical-shift tensor for each carbon in the molecule.

Table 5 Chemical-shift tensor orientation angles (°) for the δ_{11} and δ_{22} component

	C-3	C-4	C-6	C-7	C-8	C-9	C-10
δ_{11}	14.29	35.06	2.70	7.80	11.10	1.74	23.29
δ_{22}	19.37	4.96	27.08	27.41	23.25	32.58	7.913

gradient unit (50 G cm^{-1}). An inverse broadband probehead was used. A 5 mg sample of **1** was dissolved in 0.5 ml of DMSO-d_6.

Cross-polarization magic angle spinning solid state ^{13}C NMR spectra were recorded on a Bruker Avance DSX 300 spectrometer with high-power proton decoupling at 75.432 MHz for ^{13}C. A standard Bruker double-bearing 4 mm rotor system (ZrO_2 rotors, Kel–F and caps) was used. DFT GIAO calculations were carried out with the GAUSSIAN 98 program running on a Silicon Graphics Power Challenger computer. Molecular modeling calculations were performed with the HyperChem™ program also running on a Silicon Graphics Power Challenger computer. Energy minimization was carried out with the HyperChem default values. For all methods, calculations were running until the square root of the gradient vectors (RMS) were at least 0.1 kcal mol^{-1} $Å^{-1}$.

Plant material

Bidens tripartita L. herbs (1200 g) were collected near Bielsk Podlaski (Poland) in August 1997. The voucher specimen was deposited in the Department of Pharmacognosy, Medical Academy of Bialystok, Poland (No. BT 97005).

Extraction and isolation

The air dried, powdered herbs of *Bidens tripartita* were purified with petrol and $CHCl_3$ in a Soxhlet apparatus and then extracted with MeOH under reflux. The methanolic extract was successively partitioned between diethyl ether, ethyl acetate and *n*-butanol. The residue obtained after evaporation of the EtOAc extract (64 g) was chromatographed over polyamide (ROTH) with MeOH–H_2O with increasing amounts of MeOH. After crystallization from MeOH, fractions eluted with 10%–40% MeOH yielded 635 mg of compound **1**.

References

1 J. Moline, I. Bukharovich, M. Wolff and R. Phillips, *Med. Hypotheses*, 2000, **55(4)**, 306.
2 P. Pietta, *J. Nat. Prod.*, 2000, **63(7)**, 1035.
3 I. Wawer and A. Zielinska, *Magn. Reson. Chem.*, 2001, **39**, 374 and references cited therein.
4 W. S. Veeman, *Progr. Nucl. Magn. Reson. Spectrosc.*, 1984, **16**, 193.
5 A. G. Serbin, M. I. Borisov, V. T. Chernobai, I. P. Kovalev and V. G. Gordienko, *Khim. Prir. Soedin.*, 1975, **11(2)**, 144.
6 O. N. Antzutkin, S. C. Shekar and M. H. Levitt, *J. Magn. Reson.*, 1995, **115**, 7.

7 O. N. Antzutkin, Y. K. Lee and M. H. Levitt, *J. Magn. Reson.*, 1998, **135**, 144.
8 G. Metz, X. Wu and S. O. Smith, *J. Magn. Reson.*, 1994, **110**, 219.
9 A. E. Bennet, Ch. Rienstra, M. Auger, K. Lakshmi and R. Griffin, *J. Chem. Phys.*, 1995, **103**, 6951.
10 L. Frydman, G. C. Chingas, Y. K. Lee, P. J. Grandinetti, M. A. Eastman, G. A. Barral and A. Pines, *J. Chem. Phys.*, 1992, **97**, 480.
11 J. Hu, W. Wang, F. Liu, M. S. Solum, D. W. Alderman and R. J. Pugmire, *J. Magn. Reson., Ser. A*, 1995, **113**, 210.
12 J. D. W. Alderman, G. McGeorge, J. Z. Hu, R. J. Pugmire and D. M. Grant, *Mol. Phys.*, 1998, **95**, 1113.
13 A. C. Kolbert and R. G. Griffin, *Chem. Phys. Lett.*, 1990, **166**, 87.
14 O. N. Antzutkin, *Prog. NMR Spectrosc.*, 1999, **35**, 203.
15 W. T. Dixon, *J. Magn. Reson.*, 1982, **44**, 220; W. T. Dixon, *J. Chem. Phys.*, 1982, **77**, 1800.
16 J. Herzfeld and A. Berger, *J. Chem. Phys.*, 1980, **73**, 6021.
17 G. Jeschke and G. Grossmann, *J. Magn. Reson., Ser. A*, 1993, **103**, 323.
18 Z. Gu, R. Zambrano and A. McDermott, *J. Am. Chem. Soc.*, 1994, **116**, 6368.
19 D. M. Grant, J. C. Facelli, D. W. Alderman and M. H. Sherwood, *Nuclear Magnetic Shielding and Molecular Structure*, ed. J. A. Tossell, Kluwer Academic Publishers, Netherlands, 1993, pp. 367–384.
20 V. G. Malkin, O. L. Malkina, L. A. Eriksson and D. R. Salahub in, *Theoretical and Computational Chemistry*, Modern density functional theory: a tool for chemistry, 1995, J. M. Seminaro, P. Politzer (Eds.), Vol. 2, Elsevier.
21 M. J. Potrzebowski, G. Grossmann, K. Ganicz, S. Olejniczak, W. Ciesielski, A. E. Koziol, I. Wawrzycka, G. Bujacz, U. Haeberlen and H. Schmitt, *Chem. Eur. J. in press.*
22 S. Witkowski and I. Wawer, *J. Chem. Soc., Perkin Trans. 2*, 2002, 433; S. Witkowski, D. Maciejewska and I. Wawer, *J. Chem. Soc., Perkin Trans. 2*, 2000, 1471.
23 R. Bekker, E. V. Brandt and D. Ferreira, *J. Chem. Soc., Perkin Trans. 1*, 1996, 2535; R. Bekker, E. V. Brandt and D. Ferreira, *Tetrahedron*, 1999, **55**, 10005; R. Bekker, D. Ferreira, K. J. Swart and E. V. Brandt, *Tetrahedron*, 2000, **56**, 5297.
24 L. Ch. Chang, D. Chávez, L. L. Song, N. R. Farnsworth, J. M. Pezzuto and A. D. Kinghorn, *Org. Lett.*, 2000, **2**, 515; J. M. Jez and J. P. Noel, *J. Biol. Chem.*, 2002, **277**, 1361; Y. Iwase, M. Takahashi, Y. Takemura, M. Ju-ichi, C. Ito, H. Furukawa and M. Yano, *Chem. Pharm. Bull.*, 2001, **49**, 1356.
25 G. Z. Jin, Y. Yamagata and K. Tomita, *Acta Crystallogr. Sect. C*, 1990, **46**, 310; M. Rossi, L. F. Rickles and W. A. Halpin, *Bioorg. Chem.*, 1986, **14**, 55.
26 R^2 defined as:

$$R^2 = 1 - \frac{SSE}{SST}; \text{ where } SSE = \sum (Y_j - \hat{Y}_j)^2,\ SST = (\sum Y_j^2) - \frac{(\sum Y_j)^2}{n}.$$

SSE = error sum of squares; *SST* = total sum of squares.